Superfluidity and Bose-Einstein condensation in optical lattices and porous media: A path integral Monte Carlo study

Ali A. Shams and H. R. Glyde
Department of Physics and Astronomy, University of Delaware, Newark, Delaware 19716, USA
(Received 28 October 2008; revised manuscript received 24 April 2009; published 8 June 2009)

We evaluate the Bose-Einstein condensate density and the superfluid fraction of bosons in a periodic external potential using path-integral Monte Carlo methods. The periodic lattice consists of a cubic cell containing a potential well that is replicated along one dimension using periodic boundary conditions. The aim is to describe bosons in a one-dimensional optical lattice or helium confined in a periodic porous medium. The one-body density matrix is evaluated and diagonalized numerically to obtain the single boson natural orbitals and the occupation of these orbitals. The condensate fraction is obtained as the fraction of bosons in the orbital that has the highest occupation. The superfluid density is obtained from the winding number. From the condensate orbital and superfluid fraction, we investigate (1) the impact of the periodic external potential on the spatial distribution of the condensate, and (2) the correlation of localizing the condensate into separated parts and the loss of superflow along the lattice. For high-density systems, as the well depth increases, the condensate becomes depleted in the wells and confined to the plateaus between successive wells, as in pores between necks in a porous medium. For low-density systems, as the well depth increases the BEC is localized at the center of the wells (tight binding) and depleted between the wells. In both cases, the localization of the condensate suppresses superflow leading to a superfluid-insulator crossover. The impact of the external potential on the temperature dependence of the superfluidity is also investigated. The external potential suppresses the superfluid fraction at all temperatures, with a superfluid fraction significantly less than one at low temperature. The addition of an external potential does not, however, significantly reduce the transition temperature.

DOI: 10.1103/PhysRevB.79.214508 PACS number(s): 67.25.dr, 67.10.Ba, 67.85.Hj

I. INTRODUCTION

The two most remarkable properties of Bose fluids at low temperature are superfluidity and Bose-Einstein condensation (BEC). In this paper, we investigate the interdependence of BEC and superfluidity in an ordered periodic potential. London[1] first proposed the connection between these two properties in liquid helium. In contrast, the first successful quantitative theory of superfluidity—which is due to Landau[2]—does not explicitly mention BEC. Rather the Landau theory follows from three postulates: (1) a quantum liquid showing superfluidity consists of two components: a superfluid component composed of particles in the ground state, and a normal component composed of elementary excitations, (2) the elementary excitations have a phonon-roton (*P-R*) form with no free single-particle excitations with energy proportional to k^2, and (3) the superfluid component flows irrotationally and carries zero entropy. Starting with this minimal set of postulates, Landau was able to make a remarkable set of predictions, such as dissipationless flow and second sound, all of which were later verified experimentally.

It can, however, be shown that Landau's postulates follow naturally as a consequence of BEC as long as the superfluid velocity is defined as the gradient of the phase of the condensate wave function. Formally, if the condensate wave function is expressed as $\psi_0(\mathbf{r},t)=|\psi_0(\mathbf{r},t)|e^{i\phi(\mathbf{r},t)}$, the superfluid velocity is given by $v_s(\mathbf{r},t)=\frac{\hbar}{m}\nabla\phi(\mathbf{r},t)$. It immediately follows that $\nabla\times v_s(\mathbf{r},t)=0$, i.e., the flow is irrotational. Also, since no "ignorance" is associated with the single-particle state ψ_0, all the entropy must be carried by the normal component,[3] thereby recovering Landau's postulates. Elementary excitations of the *P-R* form with no free-particle-like excitations also follow from BEC.[4–6] An important corollary to the above is that, for a system to have system-wide superflow, $\phi(\mathbf{r},t)$ must be continuously connected across the whole sample. A transition from extended to localized BEC will therefore result in the loss of macroscopic superflow. The purpose of this paper is to demonstrate the loss of superflow arising from localization of BEC to disconnected islands in space by an external potential in finite-sized Bose systems.

To illustrate the impact of finite size on the condensate fraction, n_0, and the superfluid fraction, ρ_S/ρ, we consider for simplicity the ideal Bose gas. The condensate fraction of an ideal gas consisting of N bosons can be calculated analytically as shown in the Appendix. The dependence of n_0 on N is displayed in Fig. 1. An ideal Bose gas is not a superfluid in the sense that it does not satisfy the Landau criterion for superfluidity.[7] That is, if the gas is subjected to any translation or rotation with respect to the container walls, the gas is unstable to the creation of single-particle excitations that require energy, and therefore lead to energy dissipation and loss of superflow. In other words, the critical velocity is zero. However, if the ideal gas is held motionless or is assumed to be held in a metastable state, a superfluid density of the ideal gas can be defined in the usual way and the gas can be used as a simple model of superfluidity. This question is discussed in detail by Blatt and Butler.[8] With these important cautions, we evaluate the superfluid fraction of a finite-sized ideal gas of N bosons in the Appendix. The dependence of the ρ_S/ρ on N is displayed in Fig. 1. At finite N, both n_0 and ρ_S/ρ are unity at $T=0$ K. At finite N, both n_0 and ρ_S/ρ are finite at temperatures somewhat above the superfluid-normal transi-

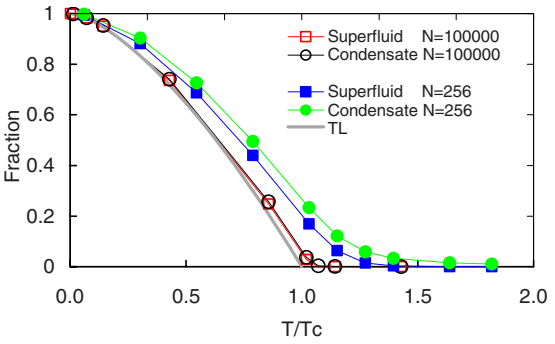

FIG. 1. (Color online) Superfluid fraction, ρ_s/ρ, and condensate fraction, n_0, of an ideal Bose gas of finite size as a function of temperature T/T_c. The size is set by the number of particles: $N=256$ and $N=100\,000$, and the thermodynamic limit (TL). T_c is the BEC critical temperature in the TL which involves the density, typically 0.1 m^{-3}. In the thermodynamic limit $n_0=N_0/N=1-(T/T_c)^{3/2}$, and n_0 and ρ_s/ρ are identical. At finite N, n_0 and ρ_s are calculated using analytic expressions given in the Appendix, and are larger than in the TL and extend to higher temperatures.

tion temperature T_c for the thermodynamic limit (TL).

In an interacting Bose fluid, the condensate fraction decreases with increasing interaction strength. In strongly interacting liquid helium the condensate fraction is only 7.25% (Refs. 9–12) but the superfluid fraction is 100% at absolute zero. However, the connection between superfluidity and BEC via the condensate wave function survives. For example, superfluidity, BEC, and well defined *P-R* excitations still all appear at the same condensation temperature[13–17] T_λ. In three dimensions superfluidity in a uniform fluid appears to be inseparably linked to the existence of BEC, a connection made in Tisza's two-fluid model of helium II. On the other hand, Kosterlitz and Thouless[18] have shown that it is possible to have superfluidity in two dimensions without BEC although the onset of superfluidity is associated with the onset of algebraically decaying long-range order.[19,20] Also the dependence of superfluidity on BEC in nonuniform systems in which the condensate may not be continuous is of great current interest,[21] the topic investigated here.

In this paper we focus on two broad classes of systems: trapped Bose gases in optical lattices (OL) and Bose liquids in porous media. The properties of bosons in external potentials and in disorder have been extensively investigated with primary focus on the nature of superfluid-insulator transition. Fisher and co-workers[22] in their seminal study of bosons on a lattice showed that, for commensurate filling of the lattice, a transition from a superfluid state to a Mott insulator (MI) state takes place at a critical ratio of the hopping strength to interparticle repulsion. Jaksch *et al.*[23] adapted these ideas to bosons confined to an optical lattice, and showed that a transition from a superfluid to MI phase is expected in OLs. The transition was first observed by Greiner *et al.*[24] using Rb^{87} atoms in a three-dimensional optical lattice. Many examples have been reported[25,26] and OLs with many atoms on a lattice site (in the potential wells at the lattice sites) have been created,[27,28] as the case considered here. Recently, OLs with disorder added have been investigated in a search for a transition from a superfluid to a Bose glass insulating phase.[29–32]

In OLs, the existence of superfluidity is inferred from the appearance of a singular peak in the atomic momentum distribution at zero momentum ($k=0$). This peak signals long-range coherence in the BEC. There remains discussion about the precise signature of extended BEC (Refs. 33 and 34) since there can be peaks at finite k without BEC in the MI state. Also, when there are many atoms per site, our results suggest that it is possible to have BEC but negligible superflow along the lattice if the BEC is highly localized in the potential wells. Some coherences in the BEC have been observed in the MI phase.[27] Our study is directed at displaying explicitly how localization of the BEC at lattice sites leads to loss of superflow along the lattice.

Equally interesting are high-density Bose liquids confined in a disordered potential—of which liquid helium in porous media[35] is a prime example. In this case, both disorder and high density introduce different physics into the interdependence of BEC (Ref. 36) and superfluidity.[35] For example, in porous media, well defined phonon-roton excitations in liquid ^{4}He are observed above the superfluid transition temperature T_c. Since *P-R* excitations imply BEC, this means that there is BEC at temperatures above T_c where there is no macroscopic superfluidity. This ostensibly goes against the widely accepted view that in an interacting system the existence of BEC implies the existence of superfluidity. The explanation proposed[37–41] is that above T_c the BEC is localized to favorable regions (e.g., larger pores) in the porous media separated by regions where depletion has brought the condensate fraction to zero. Above T_c in the porous media liquid helium contains islands of BEC separated by normal liquid. This breaking up of the BEC into isolated islands results in the loss of phase coherence across the sample and loss of superfluidity at T_c as measured by a torsional oscillator experiment. The islands of BEC still support *P-R* modes and local superfluidity. The state with BEC localized to islands is often denoted as a Bose glass. In a recent paper, Shams *et al.*[42] have shown through variational Monte Carlo (MC) simulation at 0 K that depletion-mediated localization is indeed a plausible effect in systems where there are regions of extremely high density.

The history of Monte Carlo methods in the study of Bose systems is rich and varied[10,12] although very few of these studies actually investigate superfluidity and BEC at the same time.[43] The first Monte Carlo study that simultaneously calculated both condensate fraction and superfluid density in disorder was that of Astrakharchik *et al.*[44] With weak disorder, their results agree with the Bogoliubov model.[21,45] For strong disorder their system entered an unusual regime where the superfluid fraction is smaller than the condensate fraction. Recently, Boninsegni *et al.*[43] have studied different solid phases of ^{4}He using the WORM ALGORITHM of path-integral Monte Carlo (PIMC) (the method used in the present paper). Starting from a high-temperature gas phase and "quenching" down to $T=0.2$ K, they created solid helium in a glass phase, denoted as *superglass*, i.e., a metastable amorphous solid featuring off-diagonal long-range order and superfluidity.

In the light of the above, it seemed appropriate to undertake a program whereby we simultaneously study BEC and superfluidity for a system of bosons, with the goal of inves-

tigating their interdependence. We start with the ideal Bose gas, the motivations for doing so being several: (1) the effects of interaction are absent so that the connection of BEC and superfluidity can be studied at a more fundamental level, (2) analytical expressions for both the condensate and the superfluid fractions can be obtained for a finite-sized system, which in turn can be used to check the computer code, (3) finite-size effects can be studied by comparing with the known (analytically calculated) behavior of this two quantities in the thermodynamic limit. It is seen (Fig. 1) that, for example, the condensate fraction is actually greater than the superfluid fraction for a finite-sized system (as noted above, they are *formally* identical in the TL). Also, since both of these quantities are nonzero at the critical temperature in the TL, we may conclude that the transition temperature for a finite-sized system is greater than it is in the TL (although the smoothing of the transition makes the determination of the transition temperature a bit problematic for a finite-sized system).

We then proceed to study dilute and dense interacting systems with periodic external potentials using our own PIMC code and the WORM ALGORITHM.[10,20,46] We investigate diverse low-temperature phenomena although the focus of the current paper is on the nature of BEC localization and the fate of superfluidity as BEC gets more and more localized. Specifically, we explore the condensate distribution and superfluidity in an external potential demonstrating localization of the condensate by the potential at finite temperature.

II. BOSONS IN OPTICAL LATTICE

A. Model

Our model consists of a one-dimensional (1D) lattice of potential wells. The unit cell of the lattice is shown at the top of Fig. 2. The 1D lattice is periodic along the z axis in Fig. 2. The potential is independent of x and y. For square wells, the potential within each unit cell is

$$V(x,y,z) = \begin{cases} -|V_0| & \text{for } -(b+a)/2 < z < (b+a)/2 \\ 0 & \text{elsewhere} \end{cases}, \tag{1}$$

where b is the well width parameter, a is the diameter of the hard-sphere bosons, and $|V_0|$ is the depth. Usually, $b \gg a$. The simulation is done within the unit cell only. We use periodic boundary conditions (BCs) along all directions. The periodic BC along the z direction creates the lattice. The lattice consists of thin "slabs" of attraction at regular intervals along the z direction as shown in the bottom of Fig. 2.

The specific virtue of this system is that the potential varies in one dimension only (along z). The one-body density matrix (OBDM), defined below, therefore varies along the z direction only, which enables us to diagonalize it to obtain the condensate orbitals. At the same time, since we are doing PIMC, we can also calculate the superfluid fraction along the z direction using the winding number formula.

In the present work, we consider the simplest system possible, namely, one with just one well at the center of the box (see Fig. 2). The rationale for choosing this system was gaining computational efficiency without sacrificing the essential physics. Note that the periodic nature of the potential is recovered through the use of periodic boundary conditions. In other words, what we are simulating is bosons under a periodic external potential with a periodicity of length L.

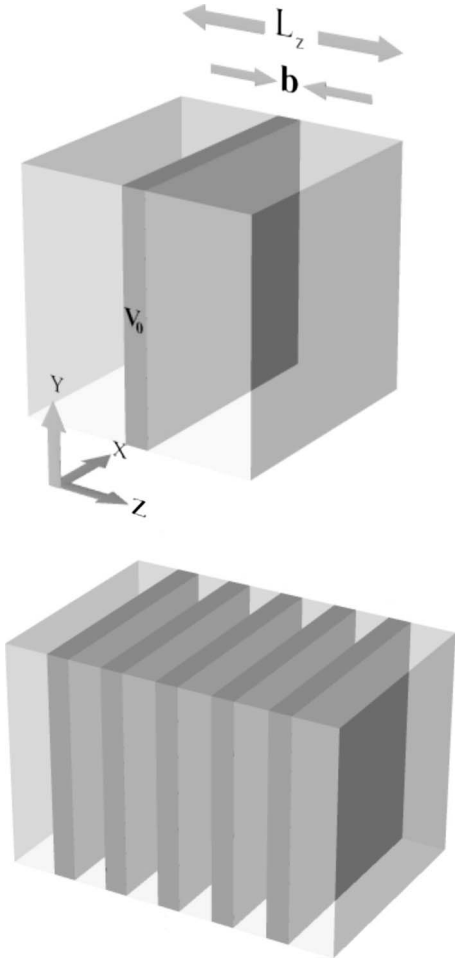

FIG. 2. Top: The cubic simulation cell containing typically 64 to 128 hard-core bosons. The darker shaded slab inside the cell represents a region of constant attractive potential of magnitude V_0. Periodic boundary conditions (PBC) are applied in all three directions. Because of the PBC along the z axis, the particles see an array of identical cubic cells along z direction as in a 1D optical lattice (bottom).

B. OBDM and single particles orbitals

1. General formulation

Following previous Monte Carlo work by DuBois and Glyde,[47] the definition we adopt for the condensate orbital in an interacting system is that given by Onsager and Penrose,[48] Löwdin,[49] and others.[50] According to this approach, the OBDM is the fundamental quantity that can be defined and evaluated for interacting systems. The single-particle orbitals and the condensate orbital in particular are defined in terms of the OBDM. The one-body density matrix is[51]

$$\rho(\mathbf{r}',\mathbf{r}) = \langle \hat{\Psi}^{\dagger}(\mathbf{r}')\hat{\Psi}(\mathbf{r})\rangle, \tag{2}$$

where $\hat{\Psi}^{\dagger}(\mathbf{r}')$ and $\hat{\Psi}(\mathbf{r})$ are the field operators for creating and annihilating a particle at $\mathbf{r}'$ and $\mathbf{r}$, respectively. The single-particle orbitals ψ_i are then be defined as

$$\rho(\mathbf{r}',\mathbf{r}) = \sum_i \psi_i^*(\mathbf{r}')\psi_i(\mathbf{r})N_i, \tag{3}$$

where N_i is the number of bosons in single-particle orbital ψ_i. The index i here is a shorthand for all the quantum numbers required to uniquely identify a single-particle orbital of the system. The condensate orbital is the single-particle orbital having the largest N_i. BEC arises if N_i is a macroscopic fraction of N. This provides a definition of BEC for finite-sized systems where there is no off-diagonal long-range order. The natural orbitals and their respective occupation numbers can be found by diagonalizing the OBDM:

$$\int\int \psi_i^*(\mathbf{r}')\rho(\mathbf{r}',\mathbf{r})\psi_i(\mathbf{r})d\mathbf{r}d\mathbf{r}' = N_i. \tag{4}$$

2. Application to the model

As described above, the external potential inside the rectangular box in our model is independent of x and y, and depends only on z. For any system uniform in x and y directions, the single-particle orbitals should have the form

$$\psi_i \equiv \psi_{mnp} = \frac{1}{\sqrt{L_x L_y}} e^{ik_m x} e^{il_n y} Z_{mnp}(z), \tag{5}$$

where m, n, and p are the state indices, and k_m and l_n are the wave numbers along x and y, determined from the boundary conditions along those directions. In this case, Eq. (4) reduces to

$$\int\int Z_{mnp}^*(z')\rho_{mn}(z',z)Z_{mnp}(z)dzdz' = N_{mnp}, \tag{6}$$

where

$$\rho_{mn}(z',z) = \int_0^{L_x}\int_0^{L_y} \rho(\mathbf{r}',\mathbf{r})\cos k_m(x'-x) \times \cos l_n(y'-y)d(x'-x)d(y'-y). \tag{7}$$

Since our goal is to find $\psi_0(\mathbf{r}) \equiv \psi_{000}(\mathbf{r})$, we only need to concern ourselves with $m=n=0$, in which case Eq. (7) becomes

$$\rho_{00}(z',z) = \int_0^{L_x}\int_0^{L_y} \rho(\mathbf{r}',\mathbf{r})d(x'-x)d(y'-y). \tag{8}$$

We evaluate $\rho_{00}(z',z)$ through Monte Carlo simulation and then numerically diagonalize it to find $\psi_0(\mathbf{r})$, that is, the single-particle orbital corresponding to the highest occupation number.

C. Superfluid fraction

In path integral Monte Carlo, each particle is represented by a "polymer," where a specific "molecule" along the polymer chain represents one specific space-time position of the particle (time in the imaginary sense), the complete polymer being the path of the particle as it "evolves" from its initial space-time position to the final one. The simulation consists in moving/changing the paths in a stochastic way, and accepting/rejecting the moves using the Metropolis condition. A "measurement" is taken of various properties after each move and the average of such properties give us the equilibrium quantum-mechanical expectation value of the properties concerned. The boundary conditions are such that the last "bead" of the polymer connects with the first one, giving us a "ring" polymer. To allow for Bose symmetry, however, the polymers are allowed to connect with each other too so that one can have very long polymers that "wind" around the box, possibly multiple times. Each such polymer has a certain "winding number" (roughly, the net number of times it winds around the boundaries in a certain direction), and the superfluid fraction is computed using the winding number formula, given by[12]

$$\frac{\rho_s}{\rho} = \frac{\langle W^2\rangle}{2\lambda\beta N}, \tag{9}$$

where W is the winding number, $\lambda = \hbar^2/2m$, $\beta = 1/k_B T$, T is the temperature, m is the mass of the bosons, and N is the total number of particles. Details of the procedure for calculating the winding number in the path-integral methodology can be found in Ref. 12, and the details of the WORM ALGORITHM of PIMC can be found in Refs. 10 and 20.

To evaluate the OBDM and ρ_S/ρ we used two PIMC codes. One, a conventional code, was written by us and used the high-temperature propagator in the primitive approximation. The second, the WORM ALGORITHM, used the high-temperature propagator in a fourth-order approximation.[45] For bosons represented by perfectly hard spheres, the fourth-order propagator effectively reduces to the primitive approximation for the interparticle interaction and is not an advantage over the primitive approximation. However, it is an advantage in those cases when the bosons are in wells that have a steep but continuous wall. To ensure convergence of the PIMC results, we increased the number of time slices, M, until the values of ρ_S/ρ, for example, did not change within 2–3 %. The number of time slices was doubled up to $M=256$. The error in ρ_S/ρ is given by the size of the points in Figs. 3–6, for example. The fluctuations in the condensate density in Fig. 3 arise from statistical error in the OBDM.

III. RESULTS

In Fig. 3 we show the superfluid fraction and the associated condensate density for bosons in the simulation cell depicted in Fig. 2 with a square well at the center of the cell. The simulation was carried out with 64 particles having helium mass and a hard-core diameter of $a=0.22a_{\mathrm{He}}$ at temperature $T=1.053T_c$. Since the mass of particles equals that of helium but the hard-core diameter is much less than the helium hard-core diameter $a_{\mathrm{He}}=2.2$ Å, what we are simulating here could be described as very weakly interacting liquid helium. The well width parameter was chosen to be $b=2.2a_{\mathrm{He}}$, and the well depth, V_0, was varied from $0.13T_c$ to

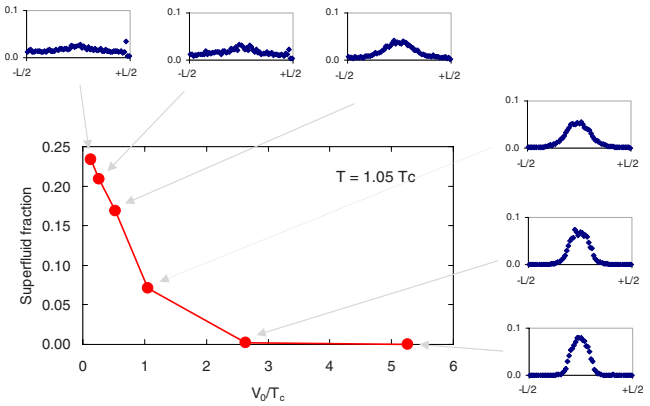

FIG. 3. (Color online) The central plot shows the superfluid fraction for flow of bosons along the 1D periodic system depicted in Fig. 2. The unit cell of side L in the 1D periodic system contains a potential well of depth V_0 at the center of the cell and ρ_s/ρ is plotted vs V_0. There are $N=64$ hard-core bosons in each cell of volume $V=L^3$. T_c is the BEC transition temperature for a uniform ideal Bose gas at the same density and mass in the TL. The satellite plots show the corresponding condensate density within a cell (in arbitrary units) along the direction of the 1D lattice. In the present example, the bosons have helium mass at a density parameter $na^3=10^{-3}$ at temperature $T=2.0$ K$=1.053T_c$ ($T_c=1.9$ K$=10.8E_R$ in TL), where E_R is the recoil energy defined in the text. In terms of the helium scattering length $a_{\mathrm{He}}=2.2$ Å, the relevant length scales are hardcore diameter $a=0.22a_{\mathrm{He}}$, well width parameter $b=2.2a_{\mathrm{He}}$, and site-to-site separation $L=8.4a_{\mathrm{He}}$. The average number density in the cell is $n=1.01\times10^{22}$ atoms/cm^3. The ratio of the hard-core diameter to site-to-site separation is $a/L=0.03$, which is typical for porous media if we take L to be the pore diameter. The parameters represent liquid helium in porous media, albeit very weakly interacting, or helium in an optical lattice. As can be seen, the superfluid fraction approaches zero as the condensate gets more and more localized at the center of each unit cell. As evidenced by the superfluid fraction ~0.25 at $V_0=0$, the system is just below its superfluid transition temperature, which is higher than the TL value due to finite-size effects.

$5.26T_c$. Since we are using periodic boundary conditions along z, we are essentially simulating a 1D array of wells with a periodicity of L_z. In all subsequent calculations the particles also have helium mass.

The main plot in Fig. 3 shows the superfluid fraction for flow along the z direction for various well depths, and the smaller plots surrounding it shows the condensate density distribution at specific values of the superfluid fraction. As can be seen, when V_0 is small, the condensate is distributed more or less evenly throughout the box and the corresponding superfluid fraction along z direction is highest. As the well depth, V_0, is increased, the condensate becomes increasingly localized around the well, and the superfluid fraction for superflow along z direction decreases. Eventually the superfluid fraction vanishes for $V_0\approx3T_c$ and the condensate density goes to near zero at the edges of the box. A strong correlation of BEC localization and the vanishing of superflow along z direction thus clearly emerges at finite temperature.

The distribution of condensate density for this system is straightforward to explain. As the well depth is increased,

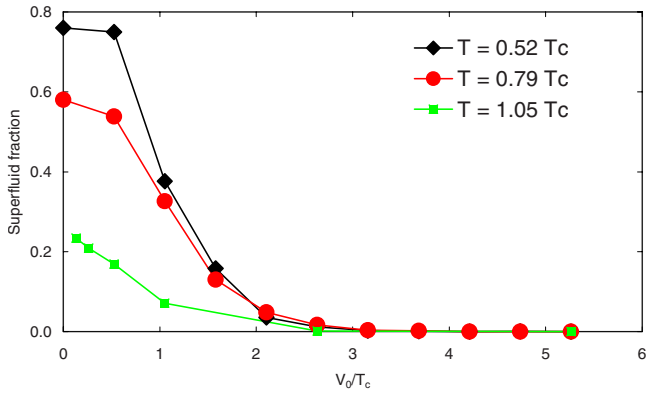

FIG. 4. (Color online) Superfluid fraction vs well depth V_0/T_c for the system shown in Fig. 3 ($na^3=10^{-3}$) at different temperatures, $T=0.53T_c$, $0.79T_c$, and $1.05T_c$, where T_c is the BEC critical temperature for a uniform Bose gas in the TL with the same particle density and mass (see Fig. 3 for further system parameters). As can be seen, the superfluid density goes to zero at approximately the same value of potential V_0/T_c independent of temperature.

particles are increasingly attracted toward the center of the box so the overall density goes up at the center. The (average) density parameter for this system is $na^3=0.001$ which is 2000 times lower than that for liquid helium. Note that although the number density for our system is quite high, it is still very weakly interacting because of the small hard-core diameter. The $na^3=0.001$ value is more characteristic of gases in optical lattices which are very weakly interacting because they are dilute and where there are similar localization effects in individual wells (see, for example, Schulte *et al.*[52]). Thus, although the number density is significantly higher at the center than it is near the edges, the system still remains sufficiently weakly interacting everywhere. This

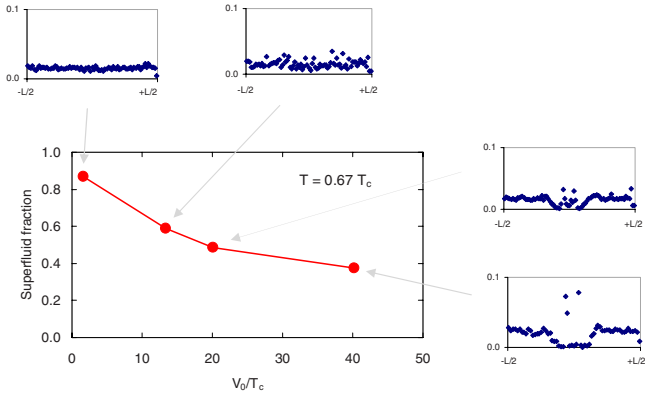

FIG. 5. (Color online) Superfluid fraction vs well depth V_0/T_c as shown in Fig. 3 but for strongly interacting bosons with large hard-core diameter $a=0.91a_{\mathrm{He}}$ and density parameter $na^3=0.16$, where $a_{\mathrm{He}}=2.2$ Å is the helium scattering length. Specifically, we simulate 128 particles having helium mass with average number density in the cell $n=2.02\times10^{22}$ atoms/cm^3. The well width parameter is $b=0.91a_{\mathrm{He}}$, (well width $b+a=2a$) and all other parameters are the same as in Fig. 3. Note that in a strongly interacting system, the condensate density is lowest at the center of the well, where the total number density is highest. The condensate is depleted by strong interaction.

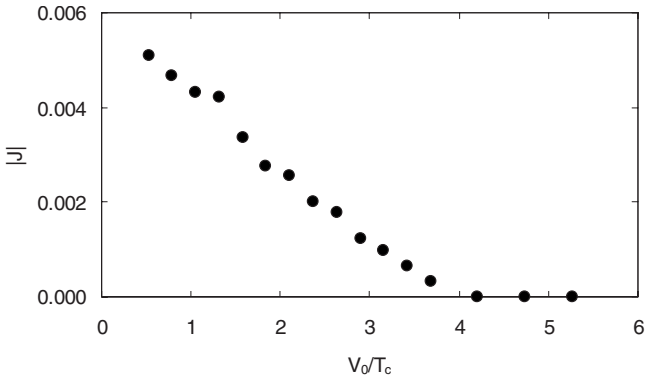

FIG. 6. The matrix element $|J|$ for hopping between sites defined in Eq. (10) (arbitrary units) vs well depth V_0/T_c for density parameter $na^3=10^{-3}$. The tunneling between sites $|J|$ decreases with increasing potential-well depth V_0 in the unit cell. T_c is the BEC critical temperature for a uniform ideal Bose gas in the TL at the same particle density and mass. J goes to zero at roughly the same V_0/T_c as the superfluid density shown in Figs. 3 and 5.

means there is no significant depletion of the condensate caused by particle correlations and the condensate density simply tracks the overall density, peaking at the center.

In this scenario, not only the condensate but particles themselves are getting localized, and successive wells are getting almost physically disconnected from each other by empty regions near the edges of the simulation box. There is no flow, let alone superflow, across the boundary of the box because there are no particles, condensed or otherwise, to carry the flow in that region. It could be said that, in this case, the loss of superfluidity is caused by a localization effect that is classical—even trivial—in nature.

To show how the suppression of superfluidity by an external potential depends on temperature, we have plotted the superfluid fraction vs V_0/T_c for three different temperatures in Fig. 4. As expected the superfluid fraction, $\rho_s(T)/\rho$, increases with decreasing temperature when V_0 is small and approaches unity at low T when $V_0=0$. At each temperature the superfluid fraction decreases with increasing V_0 and the unexpected result is that $\rho_s(T)$ goes to zero at the same value of V_0 independent of temperature. This suggests that zero-temperature calculations of the optical lattice potential needed to bring $\rho_s(T)$ to zero will be valid at finite temperatures.

Figure 5 shows $\rho_s(T)/\rho$ and the condensate density for a strongly interacting system. In this case, we simulated 128 particles of helium mass having a hard-core diameter of $a=0.91a_{\mathrm{He}}$. The square well at the center of the box had a width of $2a$ and the depth was varied from zero to approximately $40T_c$. The well in this case was therefore narrower and much stronger than in the system shown in Fig. 3. The goal was to push the density as high as possible at the center of the box so that correlation effects and depletion manifest themselves. For this system the density parameter $na^3=0.16$ is close to that in liquid helium. Again, we find the superfluid fraction to be maximum when the V_0 is small and the condensate is uniformly distributed throughout the length of the box. As the well depth is increased, the condensate distribution becomes nonuniform but in a way which is drastically different from the low-density case: the condensate is depleted in the wells where the density is high and localized primarily in the region *between* two consecutive wells. The superfluid fraction is seen to go down as the condensate gets depleted from the center but not as sharply as the low-density case. A possible explanation could be that the region of depletion is narrower than that of Fig. 3 so there is more tunneling of the condensate through the depleted region.

The reason the condensate density goes to near zero inside the well is that the extremely high number density together with a large hard-core diameter gives rise to a system that is highly correlated in that narrow strip. This results in a significant depletion of the condensate (intuitively, the more important many-body interactions become, the less the system is describable by a macroscopically occupied single-particle orbital—the definition of BEC). Outside the well, two competing effects determine the condensate density. Since the condensate density cannot exceed the total density, it has to go down as the total density goes down. However, since low density also means little depletion, we have a higher condensate *fraction*. In our case, the latter effect overrides the former, resulting in a greater condensate density outside the well than inside.

In Fig. 5, if we examine the condensate density profile at higher values of the potential depth, we notice there are spikes in the density just at the edges of the potential well. These spikes probably arise from build up of density near a perfectly hard wall when the primitive approximation is used without further correction. These spikes disappear for low density and for smoother (such as a Gaussian) potential wells. For smooth walls the fourth-order propagator that has terms depending on the derivative of the potential also becomes an advantage.

To quantify the dependence of superfluidity on the localization of BEC and to compare our results with Hubbard model calculations, we have calculated the hopping matrix element corresponding to various well depths for a low-density system. The hopping matrix element between two adjacent sites i and j, as defined by Jaksch *et al.*,[23] is given by

$$J = \int w(\mathbf{r}-\mathbf{r}_i)\left[-\frac{\hbar^2}{2m}\nabla^2 + V(\mathbf{r})\right]w(\mathbf{r}-\mathbf{r}_j)d^3\mathbf{r}, \quad (10)$$

where $w(\mathbf{r}-\mathbf{r}_i)$ is the localized Wannier orbital at site i. Since in our case, when the potential is strong, the condensate essentially separates into Wannier-type localized orbitals, the hopping matrix element as defined above can be used as a quantitative measure of the tunneling of the condensate between successive wells. The condensate orbital was first decomposed into a sum of Gaussians centered at each well, then two such consecutive orbitals were used to compute J. The result is shown in Fig. 6. As can be seen, tunneling between wells as signaled by the magnitude of J is increasingly suppressed as the well depth is increased. This is what one expects in the tight-binding regime.

In Fig. 7, we plot the superfluid fraction vs $1/J$, again for the low-density system shown in Fig. 1. Krauth *et al.*[53] have found a similar dependence of the superfluid fraction on the

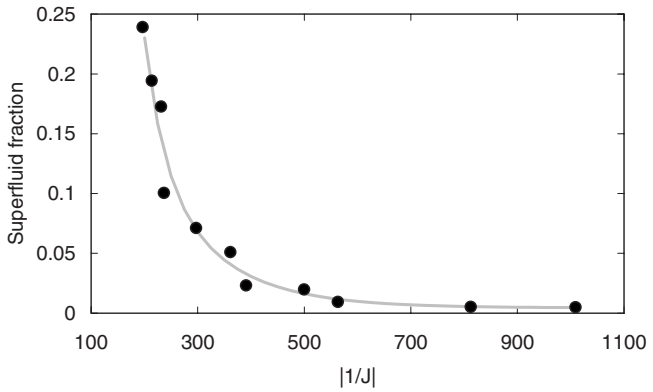

FIG. 7. Superfluid fraction vs $|1/J|$ (arbitrary units), where J is the matrix element for hopping between the sites defined in Eq. (10). The superfluid fraction falls rapidly as tunneling between adjacent sites is suppressed by increasing the potential-well depth.

interaction strength defined by U/J, where U is the on-site repulsive interaction among bosons (see Fig. 1 of Ref. 53).

Figure 8 shows the temperature dependence of the superfluid fraction, $\rho_s(T)/\rho$, for a weakly interacting system ($na^3=0.0025$) for several values of the depth, V_0, of the potential well. The observed $\rho_s(T)/\rho$ of liquid helium in different porous media is typically presented in this manner. As can be seen in Fig. 8, the external potential suppresses the $\rho_s(T)/\rho$ at all temperatures, and in contrast to a uniform system, the system is not 100% superfluid even at 0 K. The shape of the $\rho_s(T)/\rho$ curves also changes as the well depth increases with the curvature going from positive to negative around T_c. The most significant fact that emerges, however, is that all the curves approach zero at approximately the same temperature. In other words, the "transition temperature" does not seem to change with increasing well depth.

To estimate the apparent critical exponent, ζ, and superfluid transition temperature $T_c(\rho)$ of $\rho_s(T)$, we have fitted a power-law relationship to the superfluid fraction of the form

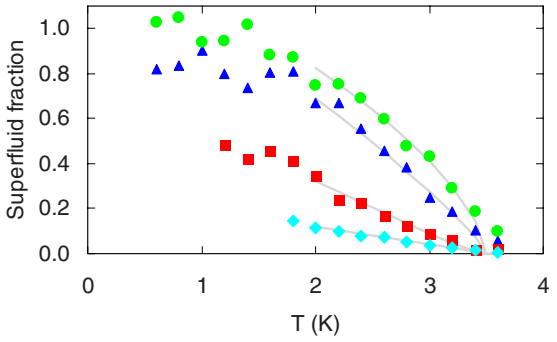

FIG. 8. (Color online) Superfluid fraction for superflow along the lattice vs T for density parameter $na^3=0.0025$, and potential-well depths in the unit cell of $V_0=0$, $1.68T_c$, $2.34T_c$, and $3.36T_c$ (top to bottom), where T_c is the BEC critical temperature for the corresponding uniform ideal Bose gas, $T_c=2.98$ K. The particle and cell parameters are: hard-core diameter $a=0.22a_{\mathrm{He}}$, well width parameter $b=2.27a_{\mathrm{He}}$, number of particles $N=128$, cell side $L=8.41a_{\mathrm{He}}$, and a Gaussian well . The solid lines are fits of $\rho_s/\rho=A[T_c(\rho)-T]^{\zeta}$. The apparent critical exponent increases from $\zeta=0.64$ for $V_0=0$ to $\zeta=1.0$ for $V_0=10$ K.

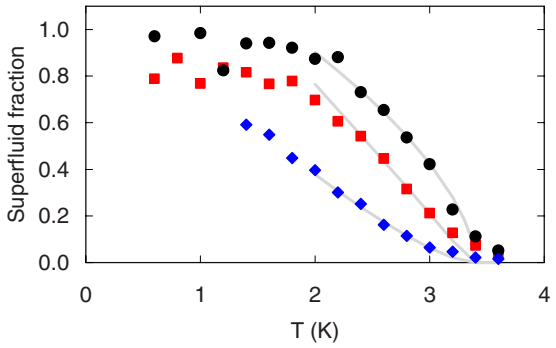

FIG. 9. (Color online) The same as Fig. 8 but with larger density parameter $na^3=0.02$. The potential-well depths are $V_0=0$, $3.36T_c$, and $6.71T_c$ (top to bottom), where T_c is the T_c for BEC in the corresponding uniform ideal Bose gas, $T_c=2.98$ K. The boson and cell parameters are: hard-core diameter $a=0.45a_{\mathrm{He}}$, well width parameter $b=2.27a_{\mathrm{He}}$, number of particles $N=128$, box side $L=8.41a_{\mathrm{He}}$, and well type=Gaussian. The fits of $\rho_s/\rho=A[T_c(\rho)-T]^{\zeta}$ to the calculated values again show an exponent ζ that increases with increasing V_0 as in Fig. 8.

$\rho_s/\rho=A[T_c(\rho)-T]^{\zeta}$ with ζ and $T_c(\rho)$ as free fitting parameters. Strictly, this power-law dependence is expected to be valid only for an infinite system very close to the critical region. This makes such a fitting problematic for a finite system because it is exactly in the critical region that $\rho_s(T)/\rho$ starts to deviate from the power-law behavior because of finite-size effects (the "tail effect"). Nevertheless, the prevailing practice is to fit the power law considerably beyond the critical region. Following this approach and to obtain values to compare with experiment, we find that the apparent ζ increases for increasing interaction, i.e., increasing well depth, V_0. Reppy[35] has observed similar behavior for liquid helium in porous media where ζ increases with decreasing porosity which implies increasing interaction with pore walls. However, ζ does not increase uniformly with decreasing pore size. For example ζ is smaller in Vycor than in aerogel. Huang and Meng[54] suggest that the apparent ζ depends on the distribution of pore sizes in the porous media and that ζ increases with increasing width in the pore size distribution. The observed $T_c(\rho)$ decreases with decreasing pore size (increasing interaction with the walls), whereas we find that $T_c(\rho)$ remains unchanged as the well depth increases.

In Fig. 9 we show $\rho_s(T)/\rho$ for several values of V_0, as in Fig. 8, for a moderately strongly interacting system ($na^3=0.02$). Qualitatively, we get the same behavior as in Fig. 8 although a much stronger potential V_0 is needed to suppress the superfluid fraction. There is a simple explanation for this in the path integral picture. For an interacting system, the particles are more resilient to clustering because of their mutual repulsion so the external potential cannot readily distort the uniform density distribution. Each particle thus always has a high number of neighbors to form macroscopic exchange cycles that gives rise to superfluidity.

IV. DISCUSSION AND CONCLUSION

The chief goal of this paper is to investigate how a periodic external potential modifies the condensate distribution

and how that in turn affects the superflow along the direction of potential variation. We used periodic boundary conditions along the z direction because we are using the winding number formula to calculate the superfluid fraction which relies on the system being periodic. Because of this periodic boundary condition we can focus on a single cell containing a potential well and the particles see an array of potential wells along the z direction. In this way our system maps directly onto those found in optical lattice experiments. For strong enough potential wells, we see localization of the condensate to islands and loss of superflow along the lattice. The localization of the condensate to islands that we see could be similar to that observed in disordered systems such as helium in porous media[37–42] because the localization in porous media is thought to be depletion mediated[41,42] rather than caused by disorder per se. Depletion can localize the condensate whenever there are sharp changes in the density profile and that can happen either in periodic or aperiodic (disordered) systems.

In high-temperature superconductors, recent measurements[55] show that, at temperatures above the superconducting transition temperature $T_c(s)$, and for certain doping levels, there can be isolated islands of superconductivity within the otherwise normal material. These islands of superconductivity exist above $T_c(s)$ up to a temperature T^* where T^* is the temperature where the evidence of Cooper pairs and an energy gap disappear. In the islands there is pairing and an energy gap. As temperature is decreased, the insulator to superconducting transition at $T_c(s)$ is associated with a crossover from separated islands of superconductivity to an extended connected superconducting state and superconductivity across the whole sample. When there are separated islands of superconductivity only, there is no superconductivity across the sample. The localization of the superconducting state to islands is believed to arise from disorder. Also in superconductors, the localization is more complicated than simple localization of the condensate to islands such as in helium in porous media case at $T_c(\rho)$ which is discussed in Refs. 37–41. It is also interesting that Ghosal *et al.*[56,57] have shown that localization of the superconducting state to islands can be induced by a homogeneous disordered potential which is a different phenomena from that considered here.

Specifically, we have shown that, for a low-density system, the condensate can be highly localized inside the potential wells of a periodic potential. Schulte[52] *et al.* have shown both experimentally and by numerically solving Gross-Pitaevskii equation that the BEC wave function in the presence of a disordered optical potential at low densities mimics a superposition of localized, and practically nonoverlapping, states. This is exactly the type of localization that we see in Fig. 3 for the deeper well values, where it is seen that the individual islands of BEC are localized in successive wells with practically zero overlap with each other. Fort *et al.*[32] have found that even in the weak-binding regime, the effect of trapping in the deepest wells cannot be avoided so the effect of disorder is mostly classical in nature, as we have found in our present simulation. To explain this, Modugno[58] did a detailed analysis of the Fort experiment using Gross-Pitaevskii theory, and reached the conclusion that one would need a shorter correlation length of the random potential than is attainable experimentally to obtain Anderson localization. In contrast, in recent experiments, Anderson localization has been observed[59,60] in optical lattices. In Anderson localization, atoms having a long wavelength are localized by incoherent scattering from many weak scattering centers.

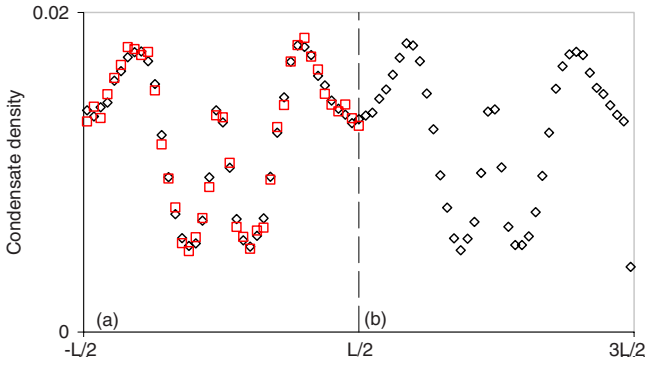

FIG. 10. (Color online) Condensate density (arb. units) vs z for a simulation box consisting of (a) 1 lattice cell with periodic boundary conditions of length L ($-L/2$ to $L/2$) (squares) and (a) + (b) 2 lattice cells with period doubled to $2L$ ($-L/2$ to $3L/2$) (diamonds). The similarity of the densities suggests that the results are not sensitive to the length of the period of the boundary conditions. The parameters are: hard-core diameter $a=0.91a_{\mathrm{He}}$, well width $b=0.91a_{\mathrm{He}}$, well depth $V_0=8.58T_c$, temperature $T=0.85T_c$, number of particles $N=178$, lattice periodicity $L=4.20a_{\mathrm{He}}$, and a Gaussian well.

An important feature of the present method is the representation of the optical lattice by the periodic images of the single well at the center of the simulation cell. Essentially, we are assuming the single-particle orbitals to have the same periodicity as that of the lattice. This is strictly true for the condensate orbital in a mean-field approximation because then the single-particle wave functions are given by the Bloch expression[61]

$$\psi_k(z) = u_k(z)\exp(ikz), \tag{11}$$

where $u_k(z)$ is a periodic function having the periodicity of the lattice, $k \equiv 2\pi s/NL_z$, N is the number of cells constituting the 1D lattice, L_z is the lattice periodicity, and $s=0,1,2\ldots,N-1$. Putting $s=0$ for the condensate orbital, we get

$$\psi_0(z) = u_0(z), \tag{12}$$

showing that $\psi_0(z)$, like $u_0(z)$, has the periodicity of the lattice.

To convince ourselves that this indeed is the case, we doubled the size of the simulation cell to consist of two cells rather than one. That is, we extended the period length of the simulation from L to $2L$ to test whether the condensate was sensitive to the period length. In Fig. 10 we compare the condensate orbitals for the two periods. The orbitals for the two periods are clearly the same showing that the orbital is insensitive to period increase from L to $2L$. By extension, simulation of a single cell plus periodic boundary conditions appears to be equivalent to simulating a full lattice.

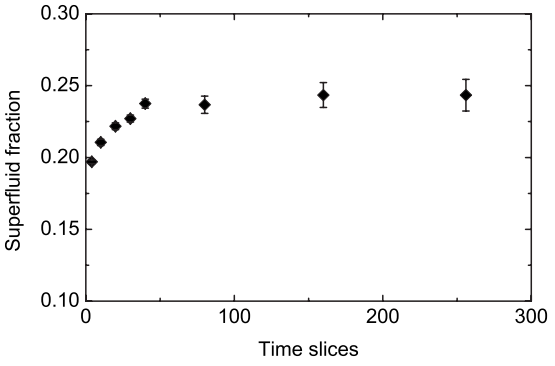

FIG. 11. Superfluid fraction for superflow along the lattice versus the number of time slices used in the PIMC calculation for the first ρ_S/ρ value shown in Fig. 3; 64 hard-core bosons at density $na^3=10^{-3}$, at temperature $T=1.053T_c$ and $V_0=0$.

The convergence of the PIMC calculations was discussed at the end of Sec. II. To illustrate convergence explicitly, we show the superfluid fraction as a function of the number of time slices used in Fig. 11. The figure shows ρ_S/ρ for 64 hard-core bosons at density $na^3=10^{-3}$, for temperature $T=1.053T_c$, and $V_0=0$, the first value of the superfluid fraction shown in Fig. 3. The ρ_S/ρ has converged to its final value at 50 time slices at this temperature and density. The convergence was similar at other values of ρ_S/ρ and at other densities.

An oft-used energy scale in optical lattice experiments is the photon recoil energy E_R, which is defined by $E_R \equiv h^2/2m\lambda^2$, where m is the mass of bosons and λ is twice the separation between wells. In terms of this quantity, $T_c=10.8E_R$ for the system shown in Fig. 3, which means the superflow almost completely vanishes at around a well depth of $30E_R$. Fertig *et al.*[62] have found that the dipole oscillations of a 1D Bose gas under a combined harmonic and optical lattice potential gets totally inhibited around a lattice well depth of $3E_R$. The much lower value they observe could be attributed to the diluteness of the gas they use. With a peak density of $n=4.7\times10^4$ cm^{-3} and a Rubidium scattering length of $a=53$ Å,[47] the density parameter in the Fertig experiment turns out to be $na^3\sim10^{-15}$. This is extremely low compared to the value of $na^3\sim10^{-3}$ for the system shown in Fig. 3. As is obvious from Fig. 5, the stronger the interaction (signified by the density parameter), the more resilient the superflow is to the inhibitory effect of the lattice potential. Schulte *et al.*[52] have also found by solving the Gross-Pitaevskii equation that the superfluid fraction of a Bose fluid in a 1D pseudorandom potential goes up with increasing strength of the interaction.

Experimentally, it is found that placing liquid helium in a disordered potential (e.g., in porous media) decreases both the critical temperature for superflow $T_c(\rho)$ and the superfluid fraction.[35,63] In Figs. 8 and 9 we show how these two quantities as calculated using PIMC change when a periodic external potential is introduced. While we do see a definite reduction in the superfluid fraction, the transition temperature $T_c(\rho)$ is apparently largely unchanged. Gordillo and Ceperley[61] have found similar results in PIMC simulation of a system of hard-core bosons in quenched disorder, i.e., when disorder is introduced $T_c(\rho)$ is largely unchanged. The conclusion could therefore be drawn that, as far as PIMC simulations of Bose fluids are concerned, the superfluid transition temperature is largely insensitive to the presence of external potentials, disordered or not.

Referring to Figs. 8 and 9, it should be mentioned that Huang and Meng[54] have called into question the standard procedure (also followed in this paper) of fitting a power-law relationship between the superfluid fraction and temperature of the form $\rho_s/\rho=A[T_c(\rho)-T]^\zeta$ when T is outside the critical region. In these authors' opinion, the different critical exponents for Vycor, aerogel, and xerogel observed experimentally are actually the result of fitting data points that are not in the critical region, and a universal critical exponent of 0.67 for all three porous media cannot actually be ruled out in the truly critical region.

ACKNOWLEDGMENTS

Valuable discussions with Massimo Boninsegni, Sui-Tat Chui, and Timothy Ziman are gratefully acknowledged. We thank Massimo Boninsegni for supplying his Worm Algorithm PIMC code. This work was supported by US DOE Grant No. DOE-FG02-03ER46038.

APPENDIX: CONDENSATE AND SUPERFLUID FRACTION FOR AN IDEAL BOSE GAS WITH A FINITE NUMBER OF PARTICLES

In this Appendix we derive the expressions for the condensate fraction, n_0, and the superfluid fraction, ρ_S/ρ, for an ideal gas of N bosons confined in a cube of volume L^3, expressions that are used to obtain the values of n_0 and ρ_S/ρ shown in Fig. 1.

1. Condensate fraction

The Bose-Einstein distribution function is given by

$$N_i=[e^{\beta(E_i-\mu)}-1]^{-1}, \tag{A1}$$

where N_i is the occupation number for the ith state, E_i is the energy of that state, μ is the chemical potential, $\beta\equiv1/k_BT$, and T is the temperature. The chemical potential μ is found from the condition

$$\sum_{i=0}^{\infty} N_i=N. \tag{A2}$$

In practice, for low temperatures, the sum over states in Eq. (A2) converges quite rapidly, and the upper limit can be replaced by a cutoff value $i_{\max}$. One then finds μ by plotting $\Sigma_{i=0}^{i_{\max}}N_i-N$ vs μ, and locating the point where the curve intersects the abscissa.

Once μ is determined, the condensate fraction follows from

$$n_0\equiv\frac{N_0}{N}=\frac{1}{N[e^{\beta(E_0-\mu)}-1]}. \tag{A3}$$

From Eq. (A3) we determine the condensate fraction for an ideal gas of N bosons in a cube of volume L^3 at uniform

density. For periodic boundary conditions, $E_0=0$. Note that n_0 depends on L through the dependence of n_0 on the higher energy eigenvalues.

2. Superfluid fraction

The superfluid fraction we use is defined in terms of the moment of inertia of the gas as[12]

$$\frac{\rho_s}{\rho} \equiv 1 - \frac{I}{I_c}, \tag{A4}$$

where I is the observed moment of inertia and I_c is the classical moment of inertia of the gas. $I_c - I$ is denoted as the nonclassical rotational inertia. The I and I_c are defined as[12]

$$I = \left. \frac{d\langle L_z \rangle}{d\omega} \right|_{w \to 0}, \tag{A5}$$

$$I_c = \sum_{i=1}^{N} \langle m_i (r_i^{\perp})^2 \rangle. \tag{A6}$$

Here, m_i is the mass of particle i, $r_i^{\perp}$ is its perpendicular distance from axis of rotation, and N is the total number of particles. The expectation value of L_z, the z component of the angular momentum, is given by[12]

$$\langle L_z \rangle = \frac{1}{Z} \sum_S \langle S | L_z e^{-\beta H_\omega} | S \rangle,$$

where $H_\omega \equiv H_0 - \omega L_z$ is the Hamiltonian in the rotating frame, H_0 is the unperturbed Hamiltonian (the perturbation being the infinitesimal angular velocity ω), Z is the partition function, and $|S\rangle$ is a many-body eigenstate corresponding to the unperturbed Hamiltonian, the summation extending over all such eigenstates. In the limit $\omega \to 0$, and with the assumption that $[H_0, L_Z]=0$ we get,

$$I = \frac{\beta}{Z} \sum_S \langle S | L_z^2 e^{-\beta E_S} | S \rangle, \tag{A7}$$

where E_S are the many-body eigenvalues of H_0. The many-body operator L_z can be expressed in terms of the single-particle creation and annihilation operators as

$$L_z = \sum_{ij} a_i^{\dagger} a_j \langle i | l_z | j \rangle, \tag{A8}$$

where l_z is the single-particle angular momentum and $|i\rangle$, $i \in \{0, 1, 2 \ldots\}$ are the single-particle energy eigenstates. With these, we have

$$I = \sum_S \sum_{ijkm} \beta \langle i | l_z | j \rangle \langle k | l_z | m \rangle \langle S | a_i^{\dagger} a_j a_k^{\dagger} a_m | S \rangle e^{-\beta E_S}.$$

Now, the factor $\langle S | a_i^{\dagger} a_j a_k^{\dagger} a_m | S \rangle$ is nonzero only in three cases: (i) $i=j=k=m$, (ii) $i=k$, $j=m$, $i \neq j$, and (iii) $i=j$, $k=m$, $i \neq k$. After some algebra, this leads to

$$I = \frac{\beta}{Z} \sum_S e^{-\beta E_S} \left\{ \sum_i l_{ii}^2 N_i^2 + \sum_{i \neq j} l_{ii} l_{jj} N_i N_j + \sum_{i \neq j} |l_{ij}|^2 N_i (1 + N_j) \right\}, \tag{A9}$$

where N_i is the occupation number corresponding to $|i\rangle$ and l_{ij} is just a shorthand for $\langle i | l_z | j \rangle$.

In the coordinate representation, we have

$$l_z \equiv (\mathbf{r} \times \mathbf{p})_z = -i\hbar \left(x \frac{\partial}{\partial y} - y \frac{\partial}{\partial x} \right), \tag{A10}$$

and for a cubic system with sides equal to L, the single-particle eigenstates are

$$|i\rangle \equiv |pqr\rangle = A e^{i(2\pi p x/L)} e^{i(2\pi q y/L)} e^{i(2\pi r z/L)}. \tag{A11}$$

Using these, it is easy to show that $l_{ii}=0$, so the first two terms inside the braces in Eq. (A9) vanish. We are thus left with

$$I = \frac{\beta}{Z} \sum_S e^{-\beta E_S} \sum_{i \neq j} |l_{ij}|^2 N_i (1 + N_j). \tag{A12}$$

Using the expressions for l_z and $|i\rangle$ given above [Eqs. (A10) and (A11)], and remembering that $\frac{1}{Z} \Sigma_S e^{-\beta E_S} N_i$ is nothing but the average number of particles $\langle N_i \rangle$ in the state $|i\rangle$, it is not too difficult to show that

$$\frac{\beta}{Z} \sum_S e^{-\beta E_S} \sum_{i \neq j} N_i |l_{ij}|^2 = \beta \frac{mL^2}{9} \sum_i \langle N_i \rangle \varepsilon_i, \tag{A13}$$

and

$$\frac{\beta}{Z} \sum_S e^{-\beta E_S} \sum_{i \neq j} N_i N_j |l_{ij}|^2 = \beta \sum_i \langle i | l_z^2 | i \rangle \langle N_i \rangle^2, \tag{A14}$$

where ε_i are the single-particle energy eigenvalues. Now, the classical moment of inertia of the cubic system is given by

$$I_c = \frac{mL^2 N}{6}, \tag{A15}$$

and with that, we finally arrive at [combining Eqs. (A4) and (A12)–(A15)]:

$$\frac{\rho_s}{\rho} = 1 - \sum_i \left[\frac{2\beta}{3N} \varepsilon_i \langle N_i \rangle + \frac{6\beta}{mNL^2} \langle i | l_z^2 | i \rangle \langle N_i \rangle^2 \right]. \tag{A16}$$

Using Eqs. (A10) and (A11), we can numerically evaluate Eq. (A15), replacing the upper limit of the summation with a cutoff value that gives us convergence to the desired degree of precision.

[1] F. London, Nature (London) **141**, 643 (1938); Phys. Rev. **54**, 947 (1938).
[2] L. D. Landau, J. Phys. (USSR) **5**, 71 (1941); **11**, 91 (1947).
[3] A. J. Leggett, Rev. Mod. Phys. **71**, S318 (1999).
[4] N. N. Bogoliubov, J. Phys. (USSR) **11**, 23 (1947).
[5] J. Gavoret and P. Nozières, Ann. Phys. (N.Y.) **28**, 349 (1964).
[6] P. Szépfalusy and I. Kondor, Ann. Phys. (N.Y.) **82**, 1 (1974).
[7] L. Pitaevskii and S. Stringari, *Bose-Einstein Condensation* (Clarendon Press, Oxford, 2003).
[8] J. M. Blatt and S. T. Butler, Phys. Rev. **100**, 476 (1955).
[9] H. R. Glyde, R. T. Azuah, and W. G. Stirling, Phys. Rev. B **62**, 14337 (2000).
[10] M. Boninsegni, N. V. Prokof'ev, and B. V. Svistunov, Phys. Rev. Lett. **96**, 070601 (2006).
[11] S. Moroni and M. Boninsegni, J. Low Temp. Phys. **136**, 129 (2004).
[12] D. M. Ceperley, Rev. Mod. Phys. **67**, 279 (1995); E. L. Pollock and D. M. Ceperley, Phys. Rev. B **36**, 8343 (1987)
[13] E. F. Talbot, H. R. Glyde, W. G. Stirling, and E. C. Svensson, Phys. Rev. B **38**, 11229 (1988).
[14] W. G. Stirling and H. R. Glyde, Phys. Rev. B **41**, 4224 (1990).
[15] H. R. Glyde, M. R. Gibbs, W. G. Stirling, and M. A. Adams, Europhys. Lett. **43**, 422 (1998).
[16] J. V. Pearce, R. T. Azuah, B. Fåk, A. R. Sakhel, H. R. Glyde, and W. G. Stirling, J. Phys.: Condens. Matter **13**, 4421 (2001).
[17] G. Zsigmond, F. Mezei, and M. F. T. Telling, Physica B **388**, 43 (2007).
[18] J. M. Kosterlitz and D. J. Thouless, J. Phys. C **6**, 1181 (1973).
[19] D. M. Ceperley and E. L. Pollock, Phys. Rev. B **39**, 2084 (1989).
[20] M. Boninsegni, N. V. Prokof'ev, and B. V. Svistunov, Phys. Rev. E **74**, 036701 (2006).
[21] K. Huang, in *Bose Einstein Condensation*, edited by A. Griffin, D. Snoke, and S. Stringari (Cambridge University Press, Cambridge, 1995), p. 31.
[22] M. P. A. Fisher, P. B. Weichman, G. Grinstein, and D. S. Fisher, Phys. Rev. B **40**, 546 (1989).
[23] D. Jaksch, C. Bruder, J. I. Cirac, C. W. Gardiner, and P. Zoller, Phys. Rev. Lett. **81**, 3108 (1998).
[24] M. Greiner, O. Mandel, T. Esslinger, T. W. Hänsch, and I. Bloch, Nature (London) **415**, 39 (2002).
[25] K. Xu, Y. Liu, J. R. Abo-Shaeer, T. Mukaiyama, J. K. Chin, D. E. Miller, W. Ketterle, K. M. Jones, and E. Tiesinga, Phys. Rev. A **72**, 043604 (2005).
[26] M. Köhl, H. Moritz, T. Stöferle, C. Schori, and T. Esslinger, J. Low Temp. Phys. **138**, 635 (2005).
[27] F. Gerbier, A. Widera, S. Fölling, O. Mandel, T. Gericke, and I. Bloch, Phys. Rev. Lett. **95**, 050404 (2005); Phys. Rev. A **72**, 053606 (2005).
[28] F. S. Cataliotti, S. Burger, C. Fort, P. Maddaloni, F. Minardi, A. Trombettoni, A. Smerzi, and M. Inguscio, Science **293**, 843 (2001).
[29] D. Clément, A. F. Varon, M. Hugbart, J. A. Retter, P. Bouyer, L. Sanchez-Palencia, D. M. Gangardt, G. V. Shlyapnikov, and A. Aspect, Phys. Rev. Lett. **95**, 170409 (2005).
[30] L. Fallani, J. E. Lye, V. Guarrera, C. Fort, and M. Inguscio, Phys. Rev. Lett. **98**, 130404 (2007).
[31] Y. P. Chen, J. Hitchcock, D. Dries, M. Junker, C. Welford, and R. G. Hulet, Phys. Rev. A **77**, 033632 (2008).
[32] C. Fort, L. Fallani, V. Guarrera, J. E. Lye, M. Modugno, D. S. Wiersma, and M. Inguscio, Phys. Rev. Lett. **95**, 170410 (2005).
[33] R. B. Diener, Q. Zhou, H. Zhai, and T.-L. Ho, Phys. Rev. Lett. **98**, 180404 (2007).
[34] Y. Kato, Q. Zhou, N. Kawashima, and N. Trivedi, Nat. Phys. **4**, 617 (2008).
[35] J. D. Reppy, J. Low Temp. Phys. **87**, 205 (1992).
[36] R. T. Azuah, H. R. Glyde, R. Scherm, N. Mulders, and B. Fåk, J. Low Temp. Phys. **130**, 557 (2003).
[37] H. R. Glyde, O. Plantevin, B. Fåk, G. Coddens, P. S. Danielson, and H. Schöber, Phys. Rev. Lett. **84**, 2646 (2000).
[38] O. Plantevin, H. R. Glyde, B. Fåk, J. Bossy, F. Albergamo, N. Mulders, and H. Schöber, Phys. Rev. B **65**, 224505 (2002).
[39] F. Albergamo, J. Bossy, P. Averbuch, H. Schober, and H. R. Glyde, Phys. Rev. Lett. **92**, 235301 (2004).
[40] F. Albergamo, J. Bossy, J. V. Pearce, H. Schober, and H. R. Glyde, Phys. Rev. B **76**, 064503 (2007).
[41] H. R. Glyde, Eur. Phys. J. Spec. Top. **141**, 75 (2007); J. Bossy, J. V. Pearce, H. Schöber, and H. R. Glyde, Phys. Rev. Lett. **101**, 025301 (2008).
[42] A. Shams, J. L. DuBois, and H. R. Glyde, J. Low Temp. Phys. **145**, 357 (2006).
[43] M. Boninsegni, N. V. Prokof'ev, and B. V. Svistunov, Phys. Rev. Lett. **96**, 105301 (2006).
[44] G. E. Astrakharchik, J. Boronat, J. Casulleras, and S. Giorgini, Phys. Rev. A **66**, 023603 (2002).
[45] K. Huang and H. F. Meng, Phys. Rev. Lett. **69**, 644 (1992).
[46] J. E. Cuervo, P.-N. Roy, and M. Boninsegni, J. Chem. Phys. **122**, 114504 (2005).
[47] J. L. DuBois and H. R. Glyde, Phys. Rev. A **63**, 023602 (2001).
[48] O. Penrose and L. Onsager, Phys. Rev. **104**, 576 (1956).
[49] P. O. Löwdin, Phys. Rev. **97**, 1474 (1955).
[50] A. J. Leggett, *Quantum Liquids: Bose Condensation and Cooper Pairing in Condensed Matter Systems* (Oxford University Press, Oxford, 2006).
[51] G. Baym, *Lectures on Quantum Mechanics* (Benjamin, London, 1976).
[52] T. Schulte, S. Drenkelforth, J. Kruse, W. Ertmer, J. Arlt, K. Sacha, J. Zakrzewski, and M. Lewenstein, Phys. Rev. Lett. **95**, 170411 (2005).
[53] W. Krauth, N. Trivedi, and D. M. Ceperley, Phys. Rev. Lett. **67**, 2307 (1991).
[54] K. Huang and H.-F. Meng, Phys. Rev. B **48**, 6687 (1993).
[55] K. K. Gomes, A. N. Pasupathy, A. Pushp, S. Ono, Y. Ando, and A. Yazdani, Nature (London) **447**, 569 (2007).
[56] A. Ghosal, M. Randeria, and N. Trivedi, Phys. Rev. Lett. **81**, 3940 (1998).
[57] A. Ghosal, M. Randeria, and N. Trivedi, Phys. Rev. B **65**, 014501 (2001).
[58] M. Modugno, Phys. Rev. A **73**, 013606 (2006).
[59] J. Billy *et al.*, Nature **453**, 891 (2008).
[60] G. Rosati *et al.*, Nature **453**, 895 (2008).
[61] C. Kittel, *Introduction to Solid State Physics*, 5th ed. (Wiley, New York, 1976), Chap. 7.
[62] C. D. Fertig, K. M. O'Hara, J. H. Huckans, S. L. Rolston, W. D. Phillips, and J. V. Porto, Phys. Rev. Lett. **94**, 120403 (2005).
[63] M. C. Gordillo and D. M. Ceperley, Phys. Rev. Lett. **85**, 4735 (2000).